Heritage Science

RESEARCH

Open Access

Hybrid nanogels and their roles in eliminating soot stains from historical paper manuscripts

Mostafa Abdel-Hamied[1*], Haidi Mahmoud Hassan[1], Yassmine Adel Mohamed[1], Mai Emad Moustafa Ismail[1], Yara Farid[1], Hager Mohamed[1], Sameh H. Ismail[2], Mohamed Z. M. Salem[3*] and Rushdya Rabee Ali Hassan[1*]

Abstract

Soot stain from diverse sources is the most common stain that stains historical paper documents found in libraries, museums, and storage facilities. It is believed to be one of the types of deterioration that arises from the contact between stains and paper sheets. Therefore, in the present work, the effectiveness of the synthesized hybrid nanogel consisting of carbopol and nanoparticles (NPs) of ZnO, TiO_2, or Fe_3O_4, in low and high-viscosity forms, for eliminating soot stains from historical paper manuscripts was conducted. The prepared hybrid nanogels were characterized utilizing the TEM, AFM, XRD, DLS, and Zeta Potential techniques. Following preparation, the soot-stained paper samples were heated to 105 °C for 6 days, a process known as accelerated thermal aging. Surface morphology, mechanical properties and the color change of the paper samples were investigated. The prepared hybrid nanogel had a spherical shape with well-defined edges and uniform size, with an average particle diameter ranging from 30 to 35 nm. There was no significant NPs agglomeration seen, suggesting uniform dispersion in the carbopol matrix. Additionally, the prepared gels' crystal structure and phase purity were revealed by the XRD analysis results. Paper fibers were visible in some parts of the treated sample with TiO_2/carbopol hybrid nanogel at high-viscosity before aging. Cleaning soot-stained paper samples using high-viscosity Fe_3O_4/carbopol hybrid nanogel is more successful than using low-viscosity nanogel. the sample treated with high-viscosity ZnONPs/carbopol hybrid nanogel produced the highest total color differences (ΔE) (26.17). The paper sample treated with high-viscosity ZnO/carbopol hybrid nanogel exhibited the maximum tensile strength (61.8 N/mm^2) and elongation at break (1.174%). The evaluation of the paper samples both before and after the cleaning process revealed that, the treatment with high-viscosity ZnO/carbopol hybrid nanogel gave the best results in removing soot stains from stained paper samples.

Keywords Paper manuscripts, Soot stains, Cleaning process, Rutile, Zincite, Magnetite, Carbopol hybrid nanogel

*Correspondence:
Mostafa Abdel-Hamied
mostafa_farag@cu.edu.eg
Mohamed Z. M. Salem
mohamed-salem@alexu.edu.eg
Rushdya Rabee Ali Hassan
rushdyarabii@cu.edu.eg
Full list of author information is available at the end of the article

Introduction

An essential element of human progress in both culture and economy is paper [1, 2]. The books, meticulously illustrated manuscripts, printing press, papers, and archival documents are priceless resources that have to be conserved and handed down to future generations [1]. In 105 AD, the Chinese invented Paper [3]. The primary source material for manuscripts, documents, publications, and graphic artworks is said to have been invented paper [4, 5].

Certain novel additives have been applied as treatments or consolidants to artifacts or model structures, where it has been demonstrated that they possess antimicrobial properties and the ability to increase strength upon cleaning [6–9]. Gellan hydrogel was used to clean four different paper samples from various periods (the XVI to the XIX) [10]. The strength of paper can be improved by strengthening additives such as synthetic, non-biodegradable polymers, the majority of which most of which pose significant concerns to human health and the environment [11]. The most respectful of the paper's original surface micromorphology are treatments of late nineteenth-century paper based on the use of rigid gels, such as agar and gellan gum, because these treatments result in the least variation in the roughness of the paper's surface when compared to brush application of cellulose ethers [12]. The components are a stiff gellan hydrogel that acts as a carrier for specific cleaning agents, such as the enzyme proteinase K, which breaks down rigid glue into smaller pieces soluble in the gel, and suitable polymeric surfactants, which have the potential to remove hydrophobic pollutants [13].

Due to different decaying factors, many paper manuscripts in different stores, libraries, and museums exhibit different kinds of stains [14, 15]. The most common stains on manuscripts are soot and other stains caused by dust, microbial contamination, etc. [16]. Soot, a black, flaky or powdery substance composed of carbon particles, is created when materials such as wood, coal, oil, etc. burn unevenly [17]. It damages manuscripts, discolors them, and becomes extremely difficult to remove because it chemically bonds the fibers of the manuscripts [18, 19].

These days, cultural asset conservation is essential for its survival because of the passage of time and exposure to various deterioration processes [20]. To preserve the original dependability of old paper and prevent damage from water use, utilizing gel to clean paper manuscripts was crucial [21, 22].

The primary goal of this research was to produce and evaluate some novel gels in the cleaning process of stained paper manuscripts with soot stains. Zinc oxide nanoparticles (ZnONPs) are characterized by an anisotropic crystal structure, luster properties, optical conductivity, motivational and oscillatory activity, high chemical and thermal stability, unsaturated surfaces, and excellent adsorption behavior towards organic and inorganic pollutants [23]. One method that shows promise for functionalizing thermosensitive materials with self-cleaning and flame-retardant qualities is applying a ZnONPs coating for low heat resistance materials, such as cotton [24]. Among the many benefits of ZnONPs are their strong antimicrobial properties and ability to self-clean surfaces, by preventing the buildup of dust or other debris [25].

Because titanium dioxide (TiO_2) is chemically inert, it has a wide range of applications. These plus the comparatively relatively inexpensive cost of the raw material and its processing led to increased interest in titania recently [26–28]. Above all, TiO_2 can absorb and scatter UV radiation in addition to being chemically resistant and having good thermal stability [29]. Because of its high photocatalytic activity, excellent optical properties, high physical and chemical stability, lack of toxicity, and high availability for practical application, TiO_2 hydrosol has been the subject of extensive research as a promising photocatalyst [30, 31]. It can also degrade adsorbed stains, bacteria, and volatile organic compounds, converting them into innocuous CO_2 and H_2O molecules [32].

Adding magnetic nanoparticles (Fe_3O_4NPs) to the gel created an excellent new approach to control it without touching the surface of the artwork or requiring the use of an extra magnet to remove any residue. An external magnet can be used to extract the magnetic nano gel from the treated surfaces, which is a significant quality that the nanogel earned [33]. In the field of conservation and other areas requiring high selectivity and control, where precise control over the release or uptake of confined material is necessary, the nano-magnetic gel functions as a smart nano-material and is the most advanced and adaptable system for cleaning artifacts [34].

It should be noted that as a result of our ongoing use of nanogels for paper cleaning, we have previously assessed the cleaning capabilities of (ZnO, TiO_2, and Fe_2O_4) carbopol hybrid nanogel in in the process of cleaning stained paper that contained dust and soil remnants [35]. In the current study, we assessed these materials in the process of cleaning soot stains from historical paper manuscripts. Every stain has a mechanism of interaction with the cleaning agents used in treatment processes, and the types of stains that need to be removed behave differently from them.

To the best of our knowledge, this is the first study that covers the entire process, including the removal of soot stains from historical paper manuscripts using carbopol hybrid nanogel made of nano-sized minerals (ZnO, TiO_2, and Fe_2O_4). These materials were chosen based on the

described nanoparticles' characteristics to be used for cleaning historical paper manuscripts in gel form.

Materials and methods

Preparation of aged stained samples

Whatman filter paper-GE Healthcare Life Sciences (CAT No. 1442–150, Model quantitative filter Whatman ashless, grade: 42, diameter: 150 mm) was used in the present study. To prepare the soot-stained paper samples, the carbon lamb was applied on the Whatman filter paper. Subsequently, to replicate the historical stained paper,, the samples of stained paper samples were subjected to accelerate thermal aging (Fig. 1A).

Synthesis of TiO_2 nanoparticles and TiO_2/carbopol hybrid nanogel

TiO_2 nanoparticles (TiO_2NPs) were synthesized by a sono-chemical method [36]. 100 mL of a 10 M NaOH solution were mixed with 0.5 g of TiO_2 powder. Using a magnetic stirrer, the liquid was continuously stirred for 4 h at room temperature while being ultra-sonicated (90% amplitude, 0.9 cycles). This resulted in the production of a precipitate containing the TiO_2NPs. The precipitate was centrifuged at 4000 rpm for 10 min and washed three times with double distilled water (DW) to eliminate impurities.

500 mL of DW was used to dissolve 1 g carbopol 940 for the nanogel production. After being dried and

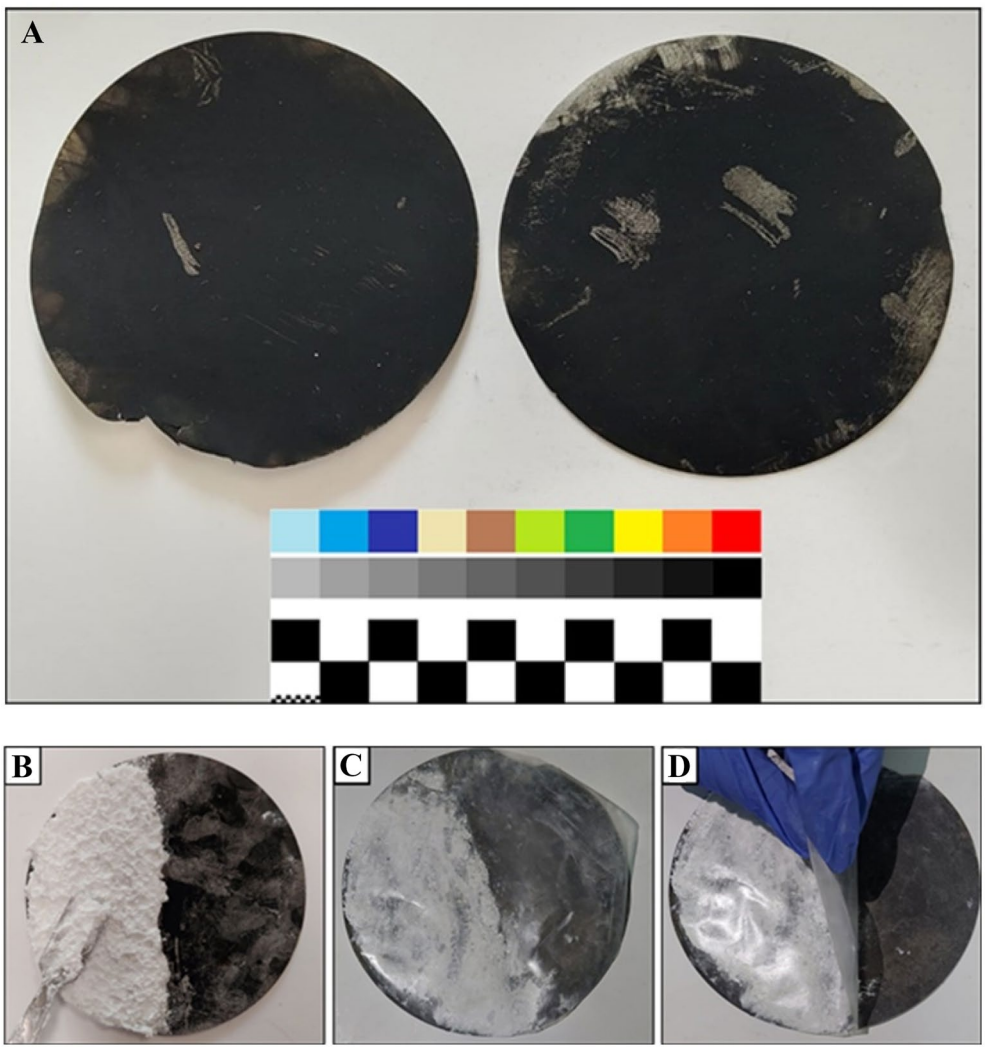

Fig. 1 Samples of paper stained with soot and the cleaning process with the prepared nano minerals (ZnO, TiO_2, and Fe_3O_4)/Carbopol Hybrid nanogel. **A** the accelerated aged stained paper samples. **B** Spatula to prepare high viscosity nanogels; **C** polyethylene sheet coverage; **D** removing gel layer with spatula

cleaned, the TiO_2NPs were added to this mixture and ultrasonically treated (90% amplitude, 90% cycle). Under continuous ultrasonication, 100 mL trimethylamine was added dropwise into this mixture, resulting in the formation of nanogel. To maximize the viscosity, the amount of trimethylamine was adjusted between 100 and 200 mL. The cross-linked carbopol matrix contained a nanogel with TiO_2NPs distributed throughout.

Synthesis of ZnO nanoparticles and ZnO/carbopol hybrid nanogel

ZnO nanoparticles (ZnONPs) were synthesized via a precipitation method [37]. In a typical procedure, a 0.2 M zinc acetate dihydrate ($Zn(CH_3COO)2{\cdot}2H_2O$) solution was prepared by dissolving the required amount in 200 mL of double-DW. The solution was subjected to ultra-sonication (Hielscher UP400S, 400 W, 24 kHz) at 80% amplitude and 0.8 cycles for 10 min while maintaining the temperature at 60 °C using a water bath. Simultaneously, ammonium hydroxide (NH_4OH, 33% w/v) was added dropwise as a precipitating agent until the reaction was completed, as evident by the appearance of a milky white precipitate. The reaction can be summarized as:

$$Zn(CH_3COO)2 + 2NH_4OH \rightarrow ZnO + 2NH_4CH_3COO + H_2O.$$

The precipitate was centrifuged at 4000 rpm for 10 min and washed three times with double-DW to remove impurities. The purified ZnONPs were dried overnight at 60 °C before further use.

For synthesizing the ZnO/carbopol hybrid nanogel, 1 g of carbopol 940 was dissolved in 500 mL of DW and combined with the dried ZnONPs. The mixture was ultra-sonicated (90% amplitude, 90% cycle), and 100 mL of trimethylamine was added dropwise under continuous ultra-sonication to induce gelation through pH change and crosslinking. The trimethylamine amount was optimized between 100 and 200 mL to obtain nanogels with the required viscosity. The nanogel was obtained as a colloidal dispersion of ZnONPs in the carbopol matrix.

Synthesis of Fe_3O_4NPs and Fe_3O_4/carbopol hybrid nanogel

Using a sono-chemical technique, magnetite nanoparticles (Fe_3O_4NPs) have been produced [38]. 0.3 g of hematite powder was added gradually to 30 mL hydrogen peroxide (H_2O_2) while being ultra-sonicated at 60 kHz using a probe sonicator (Sonica 4200 EPS3, Italy). continued For 2 h Ultra-sonication was carried out until a black precipitate that indicated the formation of Fe_3O_4NPs appeared. The Fe_3O_4NPs underwent four methanol washes to eliminate contaminants after being separated by centrifugation at 4000 rpm for 10 min.

The Fe_3O_4/carbopol hybrid nanogel was made according to the steps provided by Hassan et al. [35]. Using sonication method, 0.1 g of dried Fe_3O_4NPs were dispersed in 50 mL of ethanol. Separately, 0.5 g of carbopol was dissolved in 50 mL of ethanol. The two solutions were combined and mechanically agitated for 45 min. After 30 min, 0.5 mL of trimethylamine was added dropwise, while continuously stirred, causing nanogel to develop. Fe_3O_4NPs were dispersed throughout the cross-linked carbopol matrix to form the nanogel.

Cleaning process using the prepared carbopol hybrid nanogels

Using a spatula, high-viscosity gels were prepared (Fig. 1B), followed by covering with polyethylene sheet (Fig. 1C), and finally, the gel layer was removed with a spatula after the polyethylene sheet was removed (Fig. 1D)

Analytical techniques used for characterization of prepared nanogels

Transmission electron microscopy (TEM)

The morphology and microstructure of the nanogel were examined using a high-resolution transmission electron microscope (JEOL TEM-2100, Japan) operating at 200 kV. To prepare a diluted suspension, the samples were dispersed and ultra-sonicated in ethanol. Before imaging, a drop of this suspension was placed onto a copper TEM grid that had been coated with carbon film. It was then given time to dry completely.

Atomic force microscopy (AFM)

The nanogel samples were subjected to high-resolution 2D and 3D topographic imaging using atomic force microscopy (AFM 5600LS, Agilent, USA). Freshly cut mica sheets were employed as substrates. On the mica surface, a diluted sample suspension made according to TEM protocol was spin-coated. Aluminum-coated tips were used for contact mode imaging. The fixed scan area measured 100 nm × 100 nm.

X-ray Diffraction (XRD)

X-ray diffraction (XRD) analysis [39, 40] was carried out on a diffractometer (Philips, PANalytical X'Pert) was used to perform X-ray diffraction (XRD) examination utilizing CuKα radiation (λ = 1.5418 Å) in the 2θ range of 5–80° at a scan rate of 0.02°/s. Before being placed inside the sample holder, the nanogel samples were thoroughly dried c and ground into a fine powder using a mortar and pestle. It was maintained that the applied voltage was 40 kV and the applied current was 30 mA.

Zeta potential measurements

The zeta potential of the nanogel samples was determined using a Zeta analyzer (NanoSight NS500, Malvern Instruments Ltd., USA) equipped with a quartz cuvette containing palladium electrodes. After ultrasonicating the samples to disperse them in DW, 1 mL of this suspension was added to the cuvette. After equilibration, all measurements were performed at 25 °C with an applied current.

Dynamic light scattering (DLS)

Using NanoSight NS500 instrument (Malvern Instruments Ltd., USA), dynamic light scattering (DLS) was used to measure the hydrodynamic size distribution of the nanogels. The samples were dispersed in DW by ultrasonication. 1 mL of the diluted suspension was put into a rounded quartz cuvette that had been barium chloride-coated. At 25 °C, several replicates of the measurements were made. The intensity-weighted mean diameter was obtained by the cumulative analysis.

Analytical techniques used for evaluation of paper samples before and after treatments

Investigation of surface morphology

The surface morphology of the untreated, treated and aged samples was examined using a digital light microscope (PZ01; Shenzhen Super Eyes Co., Ltd., Guangdong, China). Further SEM examination was employed (SEM LEO 1550VP; Carl Zeiss AG, Oberkochen, Germany).

Measurement of color change

The measurement of color change for paper samples was performed by The Optimatch 3100 (Model No. CE 3100. Serial No. 31013780698, SDL Company, England) was used to measure the change in color for paper samples [14, 41].

Measurement of mechanical properties

The measurement of tensile strength (N/mm^2) and the elongation at break (%) for paper samples was carried out by H5KT, SDL Atlas, Borås, Sweden according to ISO 187 [42].

Analysis of chemical structure by ATR-FTIR

The functional groups of the chemical structure of paper samples were analyzed using the ATR-FTIR spectrometer (Model 6100, Jasco, Tokyo, Japan) both before and after cleaning procedures [43].

Cleaning mechanism of soot stains by the nanogels

The following describes how soot stain is removed from paper manuscripts using nanogel formulations.

1. The surface of the stained paper may be effectively contacted and interacted with by the nanogels because of their carbopol matrix. By weakening and expanding the stain-paper connections, the hydrated gel helps solubilize and remove the stain from the paper surface. Meanwhile, the incorporated NPs (ZnO, TiO_2, and Fe_3O_4) in the gel matrix function as cleaning agents by reacting with and dissolving the stain components.
2. Adsorption of stain compounds is made possible by the surface chemistry of the NPs, and efficient cleaning is made possible by their large surface area.
3. Probably, a blend of solubilization, physical stain detachment, photo-catalysis, and chemical interactions between NPs and stains are used in the cleaning process. When exposed to light, the photo-catalytic qualities of ZnONPs and TiO_2NPs let organic stain molecules break down into simpler, safe compounds.
4. The stain components are incorporated into the gel.
5. The application of the nanogel, which offers controlled and localized application without spreading or feathering, gently mechanically helps remove and separate the stained deposits from the paper surface.
6. The optimal penetration into stain layers and contact duration for cleaning without causing damage to the paper are ensured by the optimized viscosity.

Statistical analysis

Data of the mechanical properties [(tensile strength (N/mm^2), and the elongation at break (%)] as well as the total color change (ΔE) were statistically analyzed using one-way ANOVA. The Least Significant Difference (LSD) was used to measure the difference between means at a 0.05 level of probability.

Results and discussion

Characterization of TiO_2/carbopol hybrid nanogel

TEM and AFM microscopes were used to investigate the morphology of TiO_2NPs and their distribution and shape in the TiO_2/carbopol hybrid nanogel. The TiO_2NPs were spherical with clearly defined edges as shown by the TEM image (Fig. 2A). The average particle diameter, as determined by image analysis, was 30 ± 5 nm (mean ± SD, $n = 100$). Further insights into the nano-topography were obtained via high resolution AFM experiments. The produced NPs' spherical shape

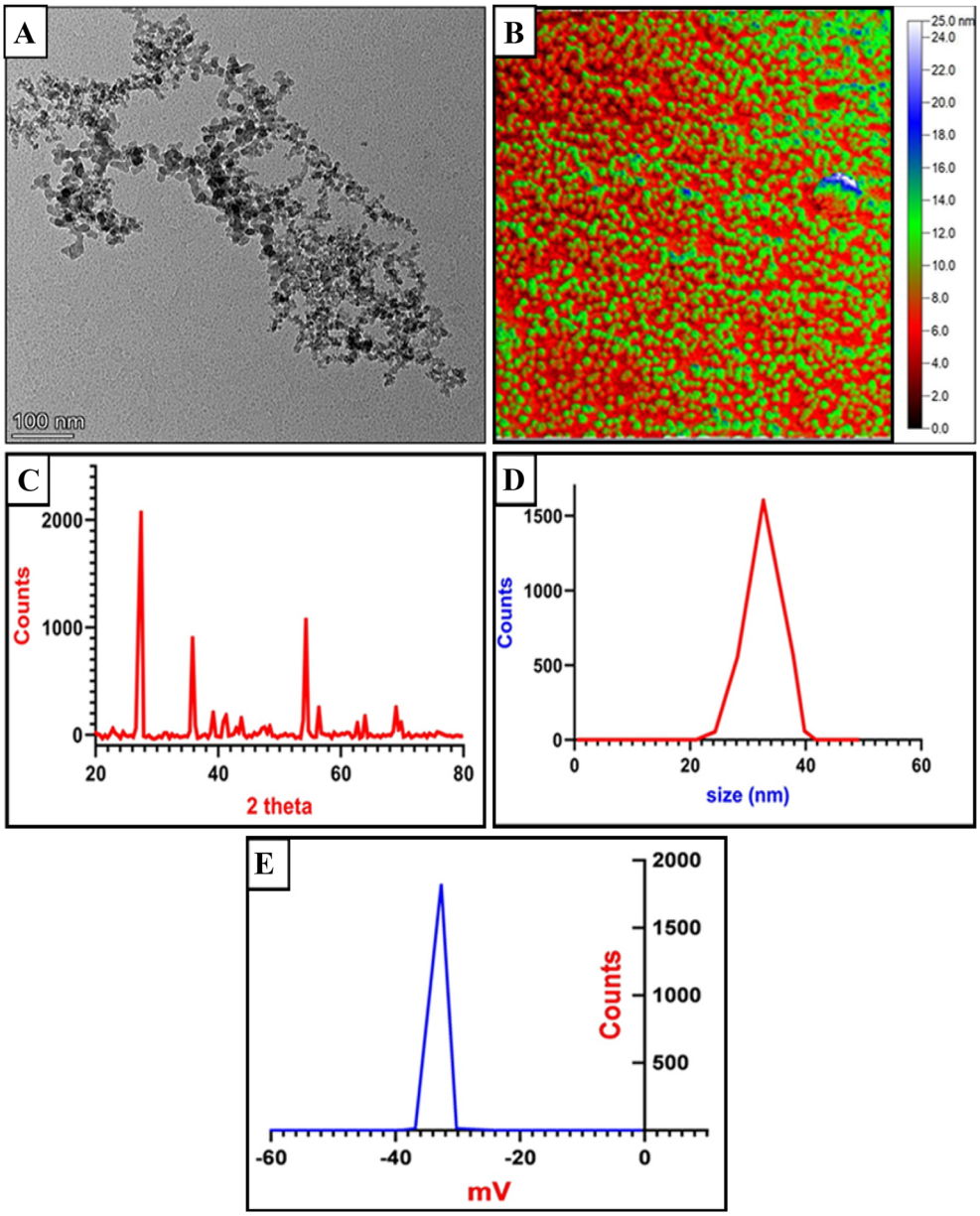

Fig. 2 Analysis of TiO_2NPs and their distribution within the TiO_2/carbopol hybrid nanogel; **A** TEM image; **B** 2D AFM image; **C** XRD pattern; **D** DLS pattern; **E** Zeta potential pattern

and size uniformity were verified by the 2D (Fig. 2B) AFM images.

The nanocomposites crystal structure and phase purity were shown by the XRD examination results (Fig. 2C). The tetragonal crystal structure of TiO_2 in the rutile phase (JCPDS 21–1276) is represented by four strong diffraction peaks at 2θ values of 27.4°, 36.1°, 41.2° and 54.3°, which are indexed to the (110), (101), (111) and (211) planes. There were no peaks of impurity found. There were no clear peaks in amorphous carbopol.

The Z-average hydrodynamic diameter of the nanogel, as determined by dynamic light scattering (DLS) tests (Fig. 2D), was 34 nm, with a low polydispersity index (PDI) of 0.212, suggesting uniform dispersion. This was consistent with the principal particle size as determined by TEM and AFM. The of As seen in (Fig. 2E), the nanogel's zeta potential was found to be -39 mV, indicating a reasonably good level of colloidal stability. Subsequently,

the TiO_2/carbopol hybrid nanogel with evenly dispersed NPs was successfully prepared, as evidenced by the TEM, XRD and DLS data.

SEM analysis by Blinov et al. [44] revealed heterogeneity and non-uniformity in SiO_2-TiO_2, TiO_2-ZrO_2 and SiO_2-ZrO_2 nanocomposite coatings evidenced by irregularities and delamination. In comparison, the present TiO_2 nanogel comprised of spherical TiO_2NPs with an average diameter of 34 nm uniformly distributed within the carbopol matrix as elucidated by TEM and DLS. This indicates significantly higher homogeneity in our nanogel system. Moreover, our study focused on heritage conservation, while Blinov et al. [44] investigated protective nanocomposite coatings for automotive paints.

Characterization of ZnO/Carbopol Hybrid Nanogel

The TEM micrographs (Fig. 3A) demonstrated the sharp edges and spherical shape of the ZnONPs. using ImageJ, software, particle size analysis revealed an average diameter of 35 ± 5 nm (mean ± SD, n = 100 particles). The spherical form was further confirmed by AFM tests (Fig. 3B). According to AFM line profiles, the particle height was around 35 nm, which agrees with the TEM measurements.

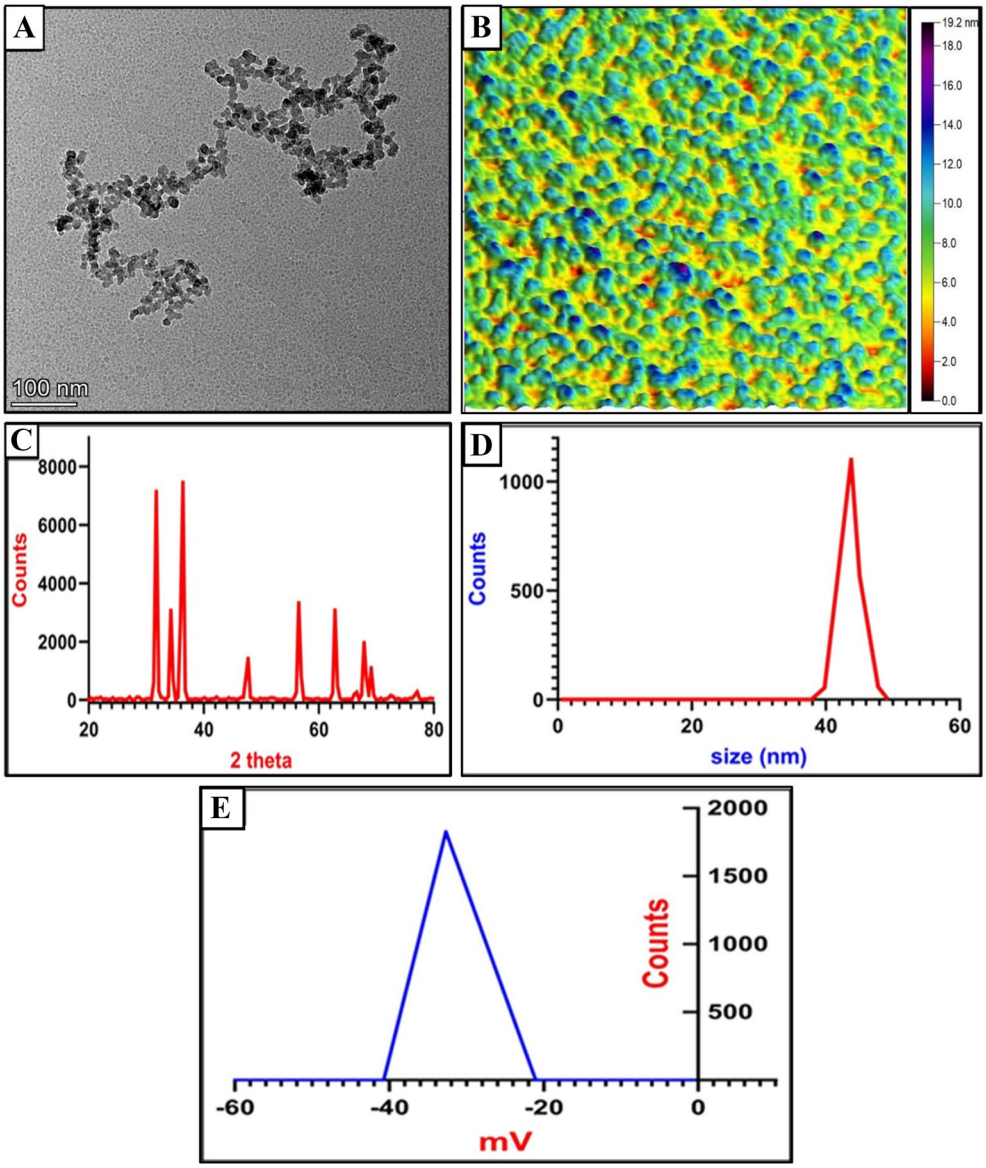

Fig. 3 Analysis of ZnO/Carbopol hybrid nanogel; **A** TEM image; **B** 2D AFM image; **C** XRD pattern; **D** DLS pattern; **E** Zeta potential

The characteristic diffraction peaks by XRD (Fig. 3C) of ZnO at 2θ displayed values of 31.9°, 34.6°, 36.4°, 47.8°, 56.9°, 63.2°, 66.7°, 68.3°, 69.4°, 72.7° and 77.4° corresponding to the (100), (002), (101), (102), (110), (103), (200), (112), (201), (004) and (202) planes, respectively, of quartzite structured ZnO (JCPDS 36–1451). There were no reactant or byproduct-related impurity peaks visible, indicating good phase purity. The diffractogram of the amorphous carbopol matrix revealed no clear peaks.

DLS was used to assess the hydrodynamic size distribution of the nanogel (Fig. 3D). With a low PDI of 0.224, the Z-average diameter was determined to be 37 nm, indicating a narrow size distribution. This exhibited a strong association with the principal particle size as determined by TEM and AFM. The zeta potential of the nanogel was -33 mV (Fig. 3E), suggesting an average degree of stability. The ionized carboxylic acid groups in carbopol are the source of the negative charge. Overall, the results from the electron microscopy, XRD and DLS showed that the ZnONPs were successfully added to the carbopol matrix, exhibiting a high dispersion stability and narrow size of distribution.

According to TEM and AFM measurements, the ZnONPs produced in this work had an average diameter of 35 ± 5 nm and a spherical shape. This is in contrast to the highly irregular shaped and polydisperse ZnONPs that are reported by Blinov et al. [45], with diameters that fall outside of the nanometer range, ranging from 150 to 1400 nm. Moreover, unlike Blinov et al. [45] who utilized biopolymer stabilization, the present ZnONPs were integrated into a carbopol gel matrix.

Characterization of Fe_3O_4/carbopol hybrid nanogel

The morphology and crystallinity of the Fe_3O_4NPs and their dispersion in the produced Fe_3O_4/carbopol hybrid nanogel were measured. The size and form of the NPs were further confirmed by TEM micrographs (Fig. 4A), which showed an average diameter of 35 nm. The absence of significant NP aggregation suggests that the particles are evenly distributed throughout the carbopol matrix. Consistent with TEM results, AFM experiments (Fig. 4B) revealed near spherical Fe_3O_4NPs, with an average height of 35 ± 5 nm estimated by line profile analysis.

The phase purity of cubic inverse spinel structured Fe_3O_4 (JCPDS 19–0629) was confirmed by the distinctive peaks at 2θ values of 30°, 35.4°, 43.03°, 53.4°, 56.91° and 62.5° that corresponded to the (220), (311), (400), (422), (511) and (440) planes, as shown in the XRD diffractograms (Fig. 4C). No impurities were detected.

The hydrodynamic diameter measured by DLS was 55 nm (Fig. 4D) with a low PDI of 0.242. The zeta potential was found to be − 24 mV (Fig. 4E), conferring moderate stability to the nanogel system. The prepared Fe_3O_4/carbopol hybrid nanogel with uniformly dispersed NPs was confirmed to have been prepared successfully by electron microscopy, XRD, and DLS characterizations. The larger size compared to microscopy measurements could be attributed to the swelling and hydration of the nanogel network.

Ba-Abbad et al. [46] showed that spherical (10 ± 2 nm) and cubic (32 ± 2 nm) Fe_3O_4NP morphologies could be achieved with NH_4OH and NaOH, respectively. On the other hand, regardless of the production technique, the present Fe_3O_4NPs showed a nearly spherical form with an average height of 35 ± 5 nm. The differing synthetic procedures can be attributable to the larger size and lack of shape selectivity. Moreover, in contrast to the free NPs produced by Ba-Abbad et al. [46], we integrated the Fe_3O_4NPs into a nanogel.

Analytical techniques used for evaluation of paper samples

Digital light microscope (USB microscope)

A substantial layer of soot stain was visible on the surface of the aged, uncleaned paper sample, as seen in the digital microscope image (Fig. 5A). Moreover, the coating of soot covering the paper surface prevents the observation of the fibers within the paper.

The fibers are not visible in the digital microscope image of cleaned sample with low-viscosity TiO_2/carbobol hybrid nanogel before aging (Fig. 5B). In comparison to the sample treated before aging, the digital microscope image of aged cleaned sample with low-viscosity nanogel (Fig. 5C) revealed that the treated sample's fibers were somewhat visible. The cleaned sample with high-viscosity nanogel before aging (Fig. 5D), showed the appearance of paper fibers, however, the majority of the fibers were not visible.

The aged cleaned sample with high-viscosity nanogel (Fig. 5E) revealed the paper's fiber fragility under a digital microscope. Compared to the control sample, the treated samples with TiO_2/carbobol hybrid nanogel at various concentrations showed improved soot layer cleaning of soot layer from the collected images; however, overall, the results were insufficient.

The data obtained for the paper sample that was treated with low-viscosity of ZnO/carbobol hybrid nanogel before aging (Fig. 5F) showed that the paper's surface white with a faint trace of soot spot residue. This demonstrates the low-viscosity gel's effectiveness. Figure 5G depicts the aged cleaned sample with low-viscosity ZnO/carbobol hybrid nanogel. The image indicates that the sample's surface remains white, indicating its resilience thermal ageing. Before aging, cleaned sample with high-viscosity ZnO/carbobol hybrid nanogel was imaged under a digital microscope (Fig. 5H), which revealed a white surface is white with

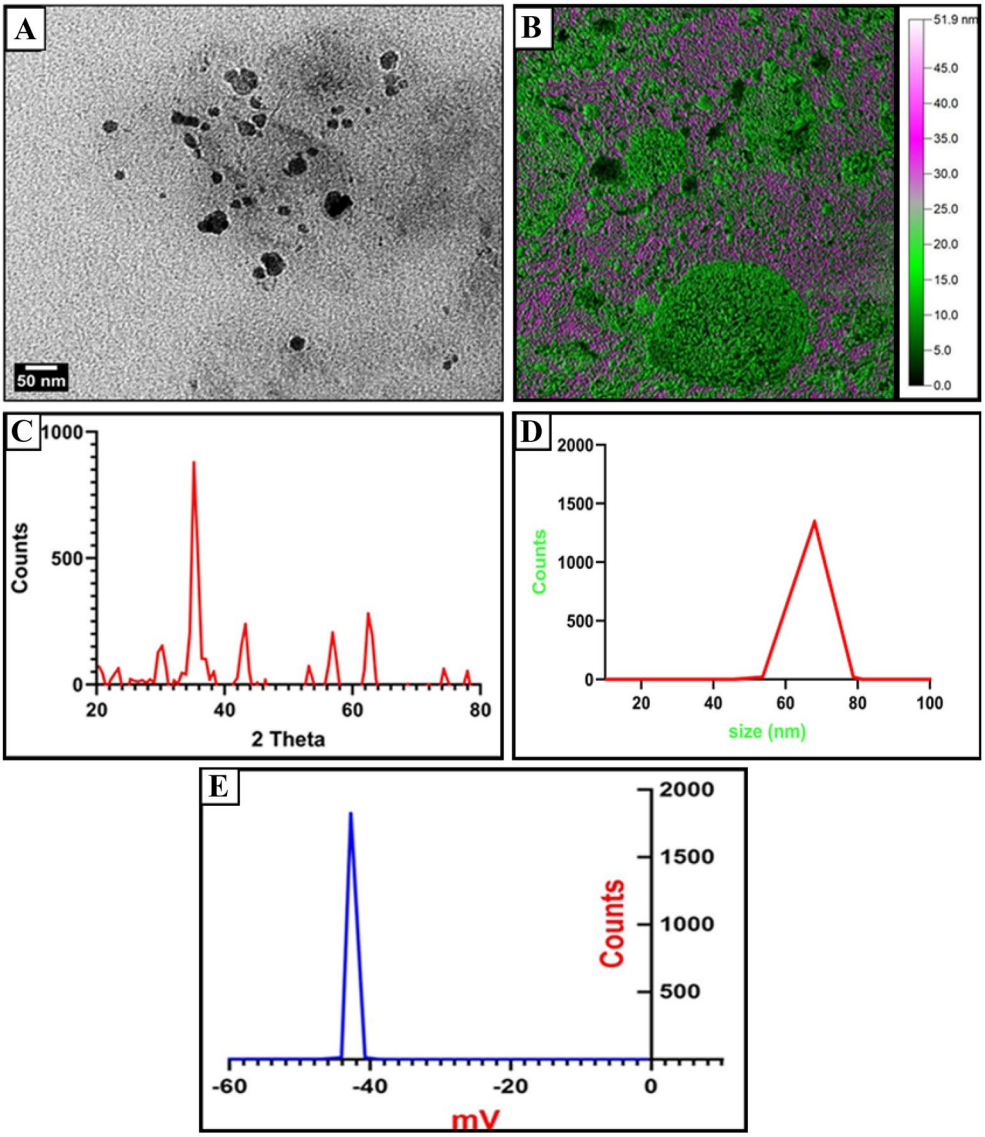

Fig. 4 Analysis of Fe_3O_4/Carbopol hybrid nanogel; **A** TEM image; **B** 2D AFM image; **C** XRD pattern; **D** DLS pattern; **E** Zeta potential

some inclusions and soot spot remnants. The surface of the aged cleaned sample with high-viscosity ZnO/carbobol hybrid nanogel (Fig. 5I) under a digital microscope revealed that the paper's fibers were still strong and its surface remained white. This outcome is related to the treated sample's resistance to thermal aging.

A trace of soot spots and certain impurities were seen in the image obtained from the cleaned sample with low-viscosity of Fe_3O_4/carbopol hybrid nanogel (Fig. 5J).

(See figure on next page.)

Fig. 5 Digital microscope image of aged soot stained sample before cleaning (**A**); **B** Cleaned sample with low viscosity TiO_2/carbopol hybrid nanogel. **C** Aged cleaned sample with low viscosity TiO_2/carbopol hybrid nanogel. **D** Cleaned sample with high viscosity TiO_2/carbopol hybrid nanogel. **E** Aged cleaned sample with high viscosity TiO_2/carbopol hybrid nanogel; **F** Cleaned sample with low viscosity ZnO/carbopol hybrid nanogel; **G** Aged cleaned sample with low viscosity ZnO/carbopol hybrid nanogel. **H** Cleaned sample with high viscosity ZnO/carbopol hybrid nanogel; **I** Aged cleaned sample with high viscosity ZnO/carbopol hybrid nanogel. **J** Cleaned sample with low viscosity Fe_3O_4/carbopol hybrid nanogel; **K** Aged cleaned sample with low viscosity Fe_3O_4/carbopol hybrid nanogel. **L** Cleaned sample with high viscosity Fe_3O_4/carbopol hybrid nanogel. **M** Aged cleaned sample with high viscosity Fe_3O_4/carbopol hybrid nanogel

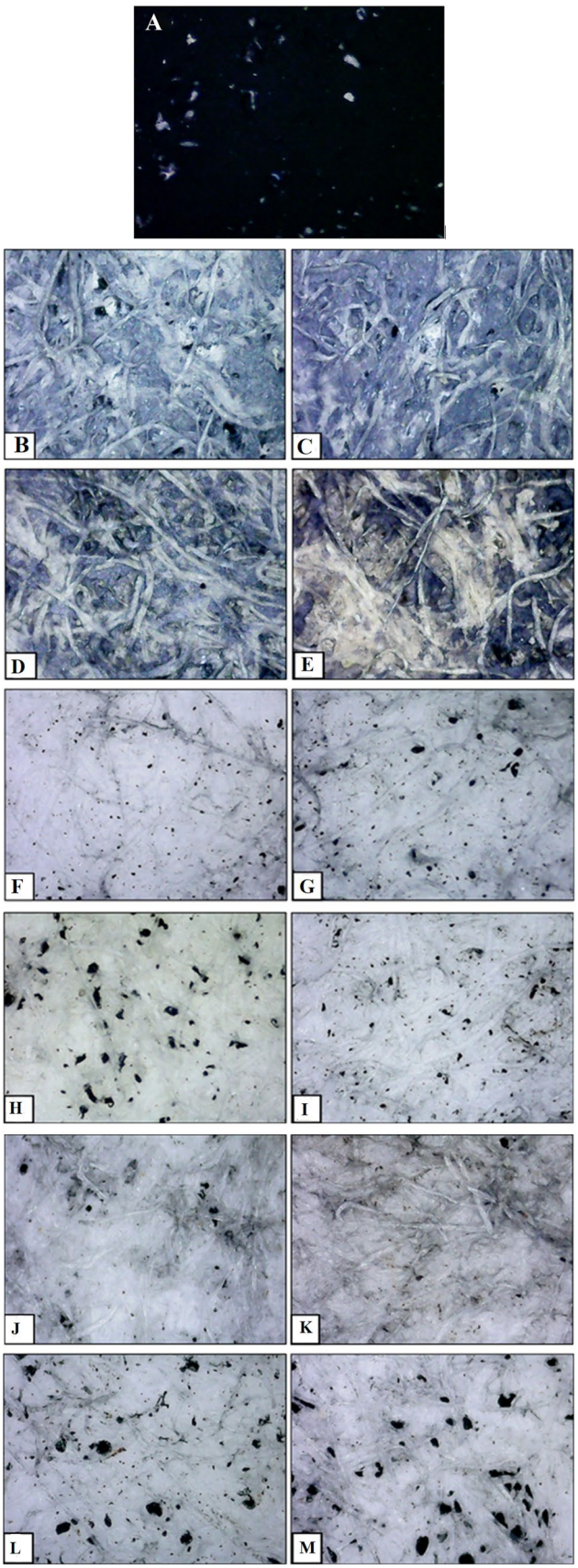

Fig. 5 (See legend on previous page.)

Furthermore, the digital image showed that the soot layer had been well cleaned, but the paper's fiber had become weak. The aged cleaned sample with low-viscosity Fe_3O_4/carbopol hybrid nanogel (Fig. 5K) revealed that the treated sample had undergone thermal aging, as seen by the darker paper fibers when compared to the treated sample before aging. The treated sample with Fe_3O_4/carbopol hybrid nanogel at low-viscosity before aging (Fig. 5L) demonstrated strong fibers despite the presence of various white patches and some soot spots in other areas places. The resistance of the treated sample with Fe_3O_4/carbopol hybrid nanogel against thermal aging was observed from the digital microscope image of the treated sample after aging process (Fig. 5M), where the paper's fibers were still strong and had not darkened.

Scanning electron microscope (SEM)

The paper sample was covered in a thick coating of soot, as seen by the SEM micrograph of soot-stained sample before cleaning (Fig. 6A). Furthermore, an obvious breakdown of the uncleaned paper's fibers was noticed after the paper sample was exposed to accelerated thermal aging, indicating an accelerated effect of thermal aging on the untreated sample's structure.

The presence of a soot layer and soot penetration into the paper's fibers was observed from the SEM micrographs of the treated sample with TiO_2/carbopol hybrid nanogel at low-viscosity before and after aging (Fig. 6B, C), however, the roughness of the surface was not apparent. Although this result indicated that the treatment was ineffective, it produced positive outcomes compared to the control sample. Paper fibers were visible in some parts of the treated sample (Fig. 6D), which was treated with TiO_2/carbopol hybrid nanogel at high-viscosity before aging. The effect of heat aging on the paper's fibers was revealed by the SEM obtained from the treated sample with TiO_2/carbopol hybrid nanogel after aging (Fig. 6E), which indicated this treated sample's low resistance against thermal aging. The SEM images (Fig. 6F, G) of the sample treated with ZnO/carbopol hybrid nanogel at low-viscosity before aging showed that the paper's fibers were in good condition, while there were some soot remains present. The fibers were visible in SEM micrographs of the treated samples with ZnO/carbopol hybrid nanogel before and after aging (Fig. 6H, I), while minor soot aggregation agglomeration was seen in some locations.

The SEM micrograph of the sample treated with Fe_3O_4/carbopol hybrid nanogel at low-viscosity before aging (Fig. 6J) revealed that the paper's fibers were destroyed, while the surface was nearly smooth from soot marks. The SEM micrograph of the aged treated sample (Fig. 6K) demonstrated the fiber fragility indicated the inadequacy of this treatment, which consequently resulted in the paper's weakness.

The paper's fibers appeared stronger than those of the treated sample with low-viscosity Fe_3O_4/carbopol hybrid nanogel, but SEM micrographs of the treated samples with Fe_3O_4/carbopol hybrid nanogel at high-viscosity before and after aging (Fig. 6L, M) revealed the existence of some soot residues. According to this study, cleaning soot-stained paper samples using high-viscosity Fe_3O_4/carbopol hybrid nanogel is more successful than using low-viscosity Fe_3O_4/carbopol hybrid nanogel.

Measurement of color change by spectrophotometer

The data in Table 1 investigated how the color characteristics (L, a, and b) and the overall ΔE of cleaned and uncleaned paper changed after 6 days of accelerated thermal aging. There were minor variations in the ΔE of the control paper in every treated sample. All treated samples provided varying values in ΔE, according to the data obtained in Table 1, but these are still good results when compared to the uncleaned sample.

The results showed that the sample treated with high-viscosity ZnONPs/carbopol hybrid nanogel produced the highest total color differences (ΔE) (26.17). This indicates that the nanogel was efficient and one of the best effective cleaning materials was used, resulting in the highest chromatic change when compared to other tested materials. These followed by the samples treated with low-viscosity ZnO/carbopol hybrid nanogel (17.91), high viscosity of Fe_3O_4/carbopol hybrid nanogel (17.78), and low viscosity of Fe_3O_4/carbopol hybrid nanogel (17.47).

Conversely, the low viscosity treated sample with TiO_2NPs/carbopol hybrid nanogel had the lowest ΔE

(See figure on next page.)

Fig. 6 SEM micrograph of aged un-cleaned paper sample before treatment (**A**); **B** Cleaned sample with low viscosity TiO_2/carbopol hybrid nanogel. **C** Aged cleaned sample with low viscosity TiO_2/carbopol hybrid nanogel. **D** Cleaned sample with high viscosity TiO_2/carbopol hybrid nanogel. **E** Aged cleaned sample with high viscosity TiO_2/carbopol hybrid nanogel. **F** Cleaned sample with low viscosity ZnO/carbopol hybrid nanogel. **G** Aged cleaned sample with low viscosity ZnO/carbopol hybrid nanogel. **H** Cleaned sample with high viscosity ZnO/carbopol hybrid nanogel. **I** Aged cleaned sample with high viscosity ZnO/carbopol hybrid nanogel. **J** Cleaned sample with low viscosity Fe_3O_4/carbopol hybrid nanogel. **K** Aged cleaned sample with low viscosity Fe_3O_4/carbopol hybrid nanogel. **L** Cleaned sample with high viscosity Fe_3O_4/carbopol hybrid nanogel. **M** Aged cleaned sample with high viscosity Fe_3O_4/carbopol hybrid nanogel

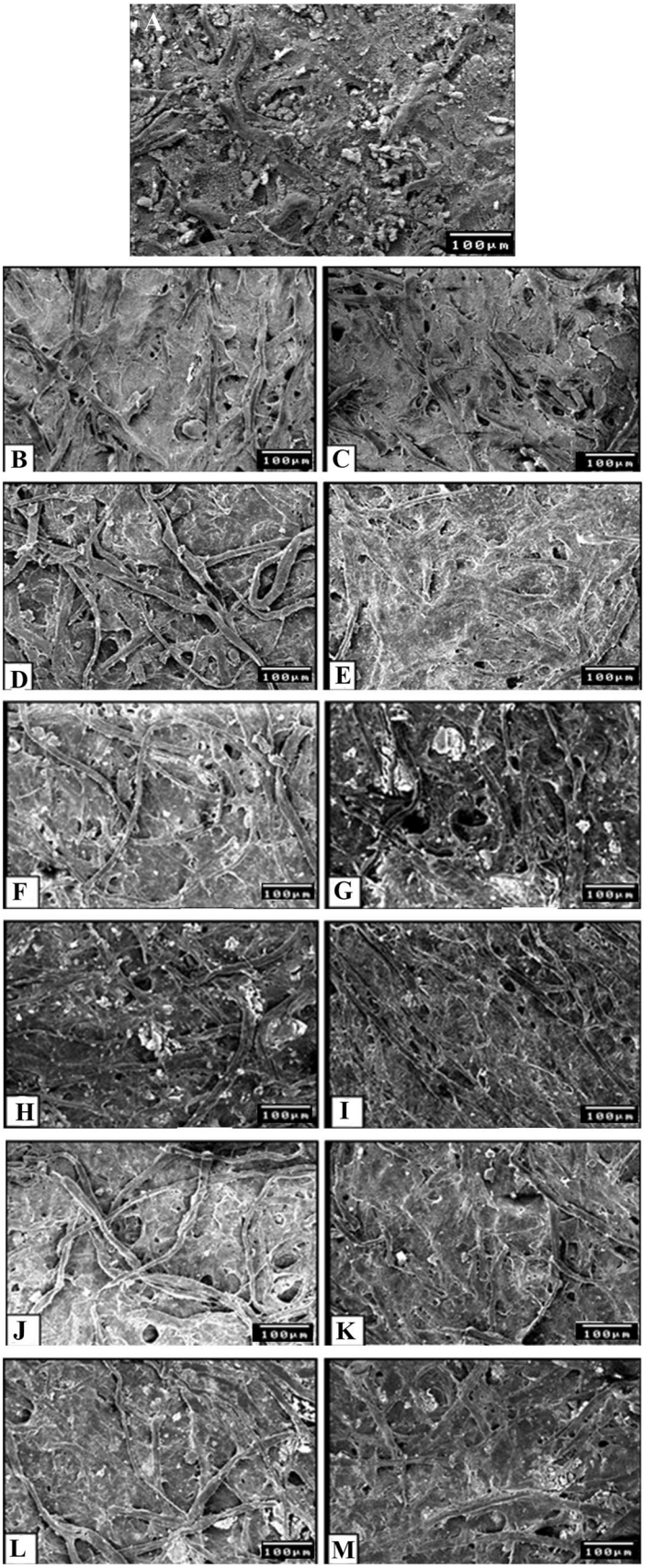

Fig. 6 (See legend on previous page.)

Table 1 The results of color change for the aged soot stained paper, treated paper and aged treated paper samples with different prepared nanogels

Samples	L	a	b	ΔE	L	a	b	ΔE
Aged stained sample before treatment	48.80	− 0.71	2.23	–	48.80	− 0.71	2.23	–
Low-viscosity nanogel					High-viscosity nanogel			
TiO_2/carbopol hybrid nanogel								
Treated sample before aging	55.49	− 0.40	1.42	6.75E ± 0.025	56.41	− 1.00	0.03	7.93E ± 0.03
Treated sample after aging	55.39	− 0.15	3.39	6.71E ± 0.02	55.49	− 0.91	0.56	6.90F ± 0.025
ZnO/carbopol hybrid nanogel								
Treated sample before aging	66.60	0.34	3.89	17.91A ± 0.02	74.94	0.21	3.29	26.17A ± 0.025
Treated sample after aging	65.63	0.09	4.35	16.97B ± 0.125	71.27	0.13	3.89	22.55B ± 0.03
Fe_3O_4/carbopol hybrid nanogel								
Treated sample before aging	65.14	0.23	3.79	16.44C ± 0.03	66.51	0.05	3.66	17.78C ± 0.02
Treated sample after aging	63.53	0.24	4.30	14.91D ± 0.02	66.26	− 0.08	2.79	17.47D ± 0.025
p-value				< 0.0001				< 0.0001
LSD 0.05				0.098				0.0465

Means with the same letter within the same column for ΔE are not significantly different according to LSD at 0.05 level of probability

value (6.75), indicating the low efficiency of the tested nanogel in comparison to the high-viscosity treated paper sample with ZnO/carbopol hybrid nanogel. A more effective cleaning solution is required to get rid of any remaining stain and restore the paper's original color if the ΔE is greater.

The primary chain scission, dehydroxylation, de-hydromethylation and dehydrogenation thermal degradation of cellulose result in the production of several free radicals that degrade and yellow the cellulose [47, 48]. By comparing the color values obtained from the aging procedure shown in Table 1, it was possible to see that none of the treatments utilized resulted in significantly different color values after aging, indicating that the materials used are stable over time. Furthermore, the low value shows that the substance is stable over time and won't have any detrimental effects on paper in the future, making this an extremely positive outcome.

Measurement of mechanical properties

Table 2 displays the results of mechanical properties (tensile strength and elongation at break) for the samples of aged treated paper, treated paper and soot-stained paper. The sample treated with high-viscosity ZnO/carbopol

Table 2 The results of mechanical properties (Tensile strength and Elongation at break) for the aged soot stained paper, treated paper and aged treated paper samples

Samples	Tensile strength (N/mm^2)	Elongation at break (%)	Tensile strength (N/mm^2)	Elongation at break (%)
Aged stained sample before treatment	29.11G ± 0.025	0.768F ± 0.002	29.11F ± 0.025	0.768G ± 0.002
Low-viscosity nanogel			High-viscosity nanogel	
TiO_2/carbopol hybrid nanogel				
Treated sample before aging	32.07E ± 0.07	0.780E ± 0.002	35.90D ± 0.02	0.908E ± 0.002
Treated sample after aging	30.1F ± 0.20	0.721G ± 0.002	35.21E ± 0.02	0.799F ± 0.002
ZnO/carbopol hybrid nanogel				
Treated sample before aging	53.9A ± 0.2	1.448A ± 0.002	61.80A ± 0.2	1.174A ± 0.002
Treated sample after aging	49.70B ± 0.015	1.291B ± 0.002	55.90B ± 0.2	1.169B ± 0.002
Fe_3O_4/carbopol hybrid nanogel				
Treated sample before aging	46.53C ± 0.02	1.052C ± 0.002	49.67C ± 0.02	1.249C ± 0.002
Treated sample after aging	46.22D ± 0.025	0.942D ± 0.002	49.58C ± 0.02	1.128D ± 0.002
P-value	< 0.0001	< 0.0001	< 0.0001	< 0.0001
LSD 0.05	0.195	0.004	0.1903	0.004

Means with the same letter within the same column are not significantly different according to LSD at 0.05 level of probability

Table 3 The characteristic function groups identified with the treated paper samples with various nanogels before and after aging process

Characteristic peaks of cellulose	TiO_2/carbopol hybrid nanogel				ZnO/carbopol hybrid nanogel				Fe_3O_4/carbopol hybrid nanogel			
	Low-viscosity		High-viscosity		Low-viscosity		High-viscosity		Low-viscosity		High-viscosity	
	Before aging	After aging	Before aging	After aging	Before aging	After aging	Before aging	After aging	Before aging	After aging	Before aging	After aging
OH	–	–	3292	3292	3281	3351	3293	3292	3349	3350	3295	3292
CH	2829	2895	–	–	2963	2841	2848	2838	2849	2855	2847	2855
C=O, C=C	–	–	1491	–	1471	–	–	–	–	–	–	–
CH	–	–	–	–	1306	1170	1306	1471	–	–	–	–
C–O–C	1066	983	1016	–	1165/993	1000	992	987	1022	1025	1023	998
O–H	–	–	805	994	765	759	776	782	780	789	775	–

– Means that the functional groups are not observed

hybrid nanogel exhibited a maximum tensile strength 61.8 N/mm^2. As a result, in comparison to other materials, it is an effective cleaning material. This was followed by the sample treated with low-viscosity ZnO/carbopol hybrid nanogel (53.9 N/mm^2), high-viscosity Fe_3O_4/carbopol hybrid nanogel (49.67 N), low-viscosity Fe_3O_4/carbopol hybrid nanogel (46.53 N/mm^2) and high viscosity TiO_2/carbopol hybrid nanogel (35.90 N/mm^2). Conversely, the sample treated with low-viscosity TiO_2/carbopol hybrid nanogel had the lowest tensile strength value (32.1 N/mm^2).

The sample treated with high-viscosity of ZnO/carbopol hybrid nanogel observed the highest elongation at break value (1.174%), suggests that the paper's mechanical properties have increased. This was followed by the sample treated with low-viscosity ZnO/carbopol hybrid nanogel (1.448%), high-viscosity Fe_3O_4/carbopol hybrid nanogel (1.249%), low-viscosity Fe_3O_4/carbopol hybrid nanogel (1.052%), and high-viscosity TiO_2/carbopol hybrid nanogel (0.909%). The sample treated with low-viscosity TiO_2/carbopol hybrid nanogel gave the lowest elongation at break value (0.78%).

When the treated paper samples' tensile strengths were compared before and after aging process, it was found that most of the results were quite near to one another. Furthermore, compared to the control (uncleaned) sample, which recorded 0.768%, it was shown that all treated samples with various nanogels, whether at high or low viscosity increased the mechanical properties of the treated paper.

Fourier transform infrared spectroscopy (FTIR)

Table 3 displays the unique functional groups present in the paper samples treated by various nanogels both before and after the aging process. The spectra of an aged, untreated paper sample (Fig. 7) revealed the presence of several distinctive soot function groups, such as C–O–C (995 cm^{-1}), and O–H (729 cm^{-1}), while, the identifiable cellulose peaks were disappeared.

The FTIR spectra of the treated sample with TiO_2/carbopol hybrid nanogel at low viscosity before aging (Fig. 7) revealed the disappearance of the most characteristic function groups of cellulose, where it was noticed CH (2829 cm^{-1}) and C–O–C (1066 cm^{-1}) [49, 50]. This confirms the result obtained from different microscopes, where this result referred to the presence of soot remains on the treated paper. FTIR spectra of the treated sample after aging (Fig. 7) showed that CH shifted from 2829 to 2892 cm^{-1} [51], which may be due to the effect of accelerated thermal aging. Additionally, the C–O–C shifted from 1066 to 983 cm^{-1} [52].

The existence of several characteristic peaks, including OH (3292 cm^{-1}), C=O (1491 cm^{-1}), C–O–C (1016 cm^{-1}), and OH (805 cm^{-1}), was seen in the FTIR spectra of the treated sample with TiO_2/carbopol hybrid nanogel at high viscosity before aging (Fig. 7). The identified function groups indicated that cellulose was present in small amounts. Moreover, the soot stain's unique peak characteristic are present.

The treated sample was affected by accelerated thermal aging, as seen by the FTIR spectra of the aged sample (Fig. 7), where two function groups were recognized as OH (3292 cm^{-1}) and C–O–C (994 cm^{-1}). This outcome is in line with the micrographs taken under various microscopes, which showed that there were remains of soot on the paper's surface.

When compared to the treated sample before aging, the FTIR spectra of the ZnO/carbobol hybrid nanogel after aging (Fig. 8) showed only minor changes, with OH (3351 cm^{-1}), CH (2841 cm^{-1}), C–O–C (1163/1000 cm^{-1}), and OH (759 cm^{-1}). When compared to the treated sample before aging, the FTIR spectra of the treated sample with ZnO/carbopol hybrid nanogel at high-viscosity before aging (Fig. 8) revealed the presence of the characteristic peaks of cellulose. such as OH (3293 cm^{-1}), CH (2848 cm^{-1}), CH (1306 cm^{-1}), C–O (992 cm^{-1}) O–H (776 cm^{-1}), and nearly disappearance of the soot characteristic peaks.

It was detected basic alterations, where OH (3292 cm^{-1}), CH (2838 cm^{-1}), C-H (1471 cm^{-1}), C–O–C (987 cm^{-1}) and O–H (782 cm^{-1}) were present as shown in the FTIR spectra of the treated paper sample after aging (Fig. 8). The FTIR spectra of the treated sample with ZnO/carbopol hybrid nanogel at low viscosity before aging (Fig. 8) revealed the presence of characteristic function groups of cellulose such as OH (3281 cm^{-1}), CH (2963 cm^{-1}), C=O (1471 cm^{-1}), CH (1306 cm^{-1}), C–O–C (1165/993 cm^{-1}), and OH (765 cm^{-1}) [53, 56].

Before aging, the sample treated with Fe_3O_4/carbopol hybrid nanogel at low viscosity provided data from FTIR analysis (Fig. 9), which revealed the existence of cellulose characteristic peaks including OH (3349 cm^{-1}), CH (2849 cm^{-1}) and C–O–C (1022 cm^{-1}). Furthermore, particular soot peaks were not seen. The effects of accelerated aging on the treated paper were shown by FTIR analysis of the treated sample after aging (Fig. 9) where shifting in position of function groups was noticed, such as OH shifted from 3349 to 3350 cm^{-1}, CH shifted from 2849 to 2855 cm^{-1}, C–O–C shifted from 1022 to 1025 cm^{-1} and O–H shifted from 780 to 789 cm^{-1}.

The FTIR spectra of the treated sample with Fe_3O_4/carbopol hybrid nanogel at high viscosity before aging (Fig. 9) revealed the presence of some characteristic peaks of cellulose such as OH (3265 cm^{-1}); CH (2847 cm^{-1}); C–O–C (1023 cm^{-1}) and O–H (775 cm^{-1}) [54]. Furthermore, certain function groups such as C=O

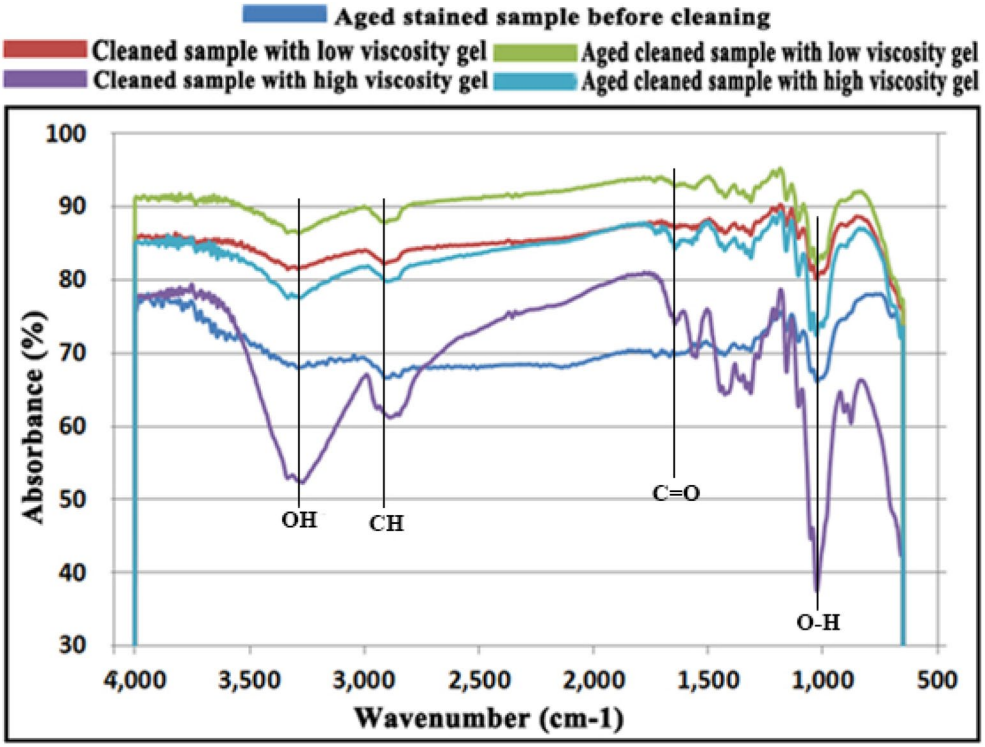

Fig. 7 FTIR spectra of control, treated and aged treated paper sample with TiO_2/carbopol hybrid nanogel at different concentrations

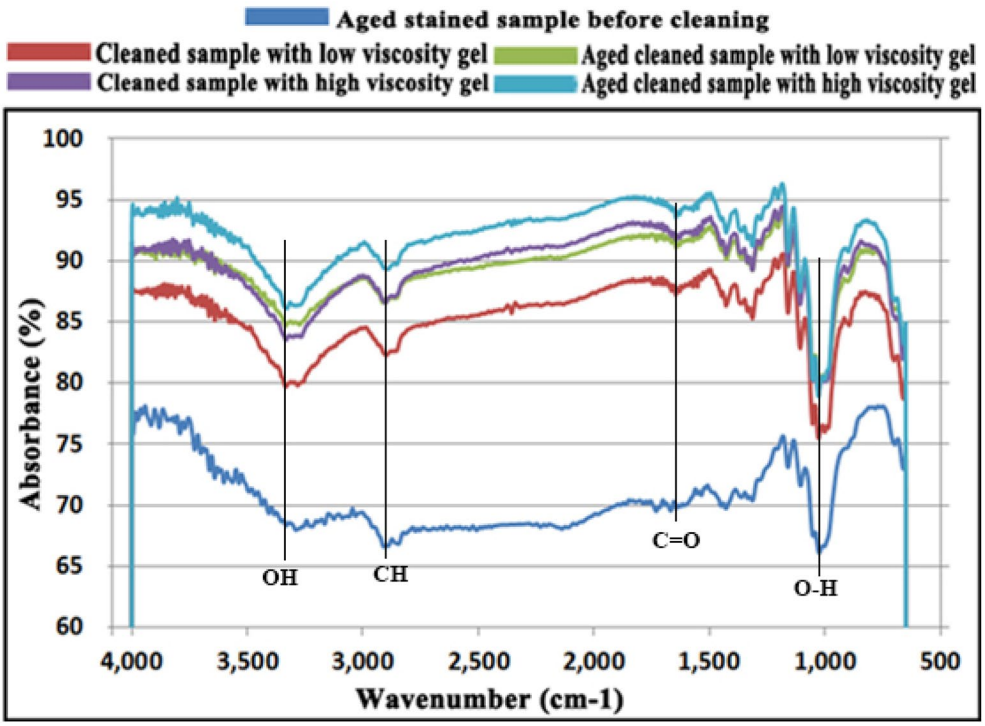

Fig. 8 FTIR spectra of control, treated and aged treated paper sample with ZnO/carbopol hybrid nanogel at different concentrations

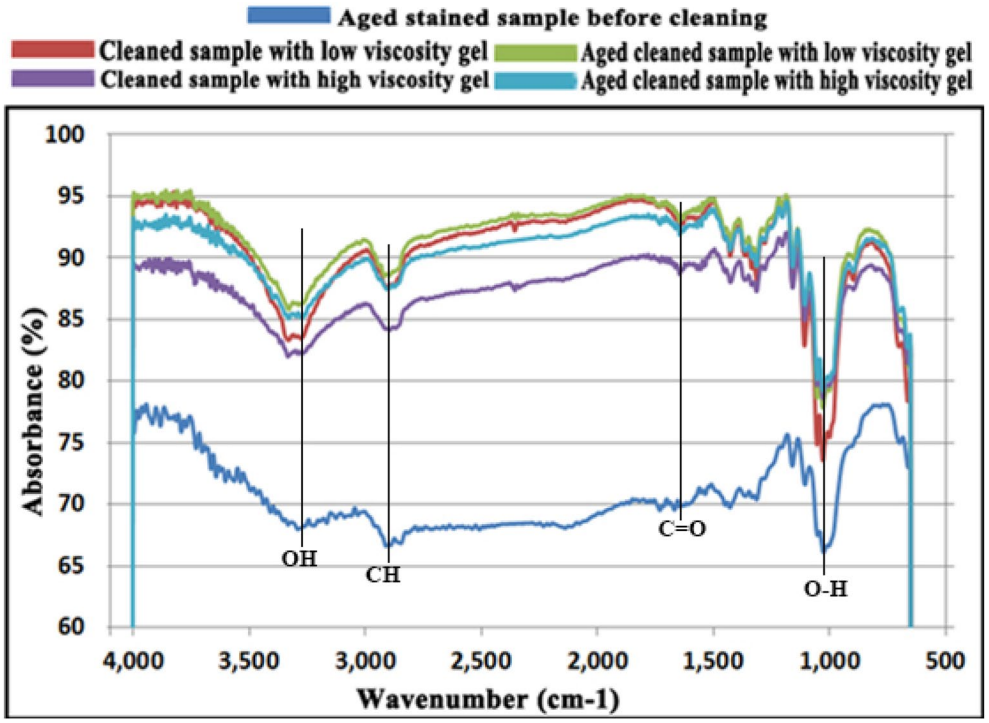

Fig. 9 FTIR spectra of control, treated and aged treated paper sample with Fe_3O_4/carbopol hybrid nanogel at different concentrations

and CH were disappeared. A small amount of soot residue was visible on the surface based on the FTIR data, which was confirmed by the results from digital and SEM microscopes. Comparing the treated sample before aging to the treated sample after aging, the FTIR of the treated sample (Fig. 9) revealed modest alterations, with OH appearing at 3292 cm^{-1}, CH at 2855 cm^{-1}, and C–O–C at 998 cm^{-1}.

It is evident from the mechanical properties, color chances and shifting in functional chemical groups that soot stains lead to a reduction in the tensile strength and elongation at break of the material. ZnO/carbopol hybrid nanogels showed effective paper-cleaning capabilities.

It was noted that symptoms of brittleness, hardness, corrosion, and discoloration were documented from parchment scrolls were polluted with different types of dirt deposits and because of inappropriate variables present in museums, storage facilities, and libraries [16]. On the surface of the paper, the ZnO cellulosic nanocomposite demonstrated an effective protective layer against the damaging effects of UV radiation, polluting gasses, mold, and bacteria [55].

From the above experimental work, when it comes to rough and uneven paper surfaces, the accuracy of spectral and imaging approaches may be compromised. Sufficient confirmation of cleaning capabilities was obtained through mechanical testing, colorimetry, and visual evaluation to meet the objectives of this proof-of-concept study. However, there are some limitations. For example, rather than measuring the precise amount removed, the focus was mostly on describing the nanogel compositions and showcasing their capacity to observably decrease soot spots. It was unable to conduct the repeated tests required for the statistical analysis of clearance rates because it had insufficient heritage paper samples to deal with. Furthermore, numerous uncontrollable variables are introduced throughout the staining and cleaning operations, which impact measurement. Stain removal quantification might have needed chemical extraction or destructive samples, which weren't feasible for rare manuscripts.

Conclusion

Because of the properties of the nano-sized minerals (ZnO, TiO_2, and Fe_2O_4) and carbopol hybrid nanogel, it can be said that this study is the first to cover the entire process, including the removal of soot stains from historical paper documents. Using various analytical techniques, the produced nanomaterials (ZnO, TiO_2, and Fe_2O_4)/carbopol hybrid nanogel have first been analyzed. The size of the nanomaterials was found to range between 30 and 35 nm, according to the results of the analytical techniques used for characterization (TEM, AFM, XRD, DLS, and Zeta Potential). Furthermore, the

well-distributed nanomaterials in the carbopol hybrid nanogel were found. Additionally, the produced gels' crystal structure and phase purity were observed. The paper sample treated with high-viscosity ZnO/carbopol hybrid nanogel produced the highest ΔE (26.17), indicating that it was an efficient and very effective cleaning material. The highest tensile strength was demonstrated by the paper sample treated with high-viscosity ZnO/carbopol hybrid nanogel. Based on the examination of the methodologies employed to assess the removal of soot stain from paper samples, it was found that the paper sample treated with ZnO/carbopol hybrid nanogel at high viscosity produced the best results in the majority of the analytical procedures employed in this inquiry. Additionally, as ZnO/carbopol hybrid nanogel has shown its effectiveness in cleaning soot stains on stained paper manuscripts, we advise employing it at high viscosity to remove the stains. In addition to providing scientific support for the cleaning, conservation, or restoration of the historical paper document, this study may provide methodological guidance based on a variety of analytical approaches.

Acknowledgements
The authors would like to extend their appreciation to the scientific cooperation among the Department of Conservation, Faculty of Archaeology, Cairo University; the Faculty of Nanotechnology for Post Graduates, Cairo University, El-Sheikh Zayed, and the Forestry and Wood Technology Department, Faculty of Agriculture (El-Shatby), Alexandria University.

Author contributions
RRAH and MA-H, wrote the main manuscript text, HMH, YAM, MEMI, YF and HM prepared figures, SHI wrote the scientific methodology of the research, RRAH, MA-H and MZMS writing–review & editing, RRAH and MA-H, MZMS, and SHI investigated the results. All authors perfectly reviewed the manuscript.

Funding
Open access funding provided by The Science, Technology & Innovation Funding Authority (STDF) in cooperation with The Egyptian Knowledge Bank (EKB).

Data availability
No data was used for the research described in the article.

Declarations

Competing interests
The authors declare that they have no competing interests.

Author details
[1]Conservation Department, Faculty of Archaeology, Cairo University, Giza 12613, Egypt. [2]Faculty of Nanotechnology for Postgraduate Studies, Sheikh Zayed Campus, Cairo University, 6th October City, Giza 12588, Egypt. [3]Forestry and Wood Technology Department, Faculty of Agriculture (El-Shatby), Alexandria University, Alexandria 21545, Egypt.

Received: 8 January 2024 Accepted: 14 March 2024
Published online: 29 March 2024

References

1. Ardelean E, Bobu E, Niculescu G, Groza C. Effects of different consolidation additives on ageing behaviour of archived document paper. Cell Chem Technol. 2011;45(1–2):97–103.
2. Abdel-Hamied M, Hassan RRA, Salem MZM, Ashraf T, Mohammed M, Mahmoud N, et al. Potential effects of nano-cellulose and nano-silica/polyvinyl alcohol nanocomposites in the strengthening of dyed paper manuscripts with madder: an experimental study. Sci Rep. 2022;12(1):19617.
3. Hassan RRA, Ali MF, Fahmy A-GA, Ali HM, Salem MZM. Documentation and evaluation of an ancient paper manuscript with leather binding using spectrometric methods. J Chem. 2020;2020:6847910.
4. Ahmed Eldeeb HM, Ali MF, Mansour MMA, Ali Ahmed MA, Salem MZM. Monitoring the effects of fungi isolated from archival document on model albumen silver prints. Microb Pathogen. 2022;169: 105632.
5. Mansour MMA, Salem MZM. Poultices as biofilms of titanium dioxide nanoparticles/carboxymethyl cellulose/Phytagel for cleaning of infected cotton paper by *Aspergillus sydowii* and *Nevskia terrae*. Environ Sci Pollut Res. 2023;30(53):114625–45.
6. Afifi HAM, Mansour MMA, Hassan AGAI, Salem MZM. Biodeterioration effects of three *Aspergillus* species on stucco supported on a wooden panel modeled from Sultan al-Ashraf Qaytbay Mausoleum. Egypt Sci Rep. 2023;13(1):15241.
7. Mansour MMA, Mohamed WA, El-Settawy AAA, Böhm M, Salem MZM, Farahat MGS. Long-term fungal inoculation of *Ficus sycomorus* and *Tectona grandis* woods with *Aspergillus flavus* and *Penicillium chrysogenum*. Sci Rep. 2023;13(1):10453.
8. Mohamed HM, Ahmed NM, Mohamed WS, Mohamed MG. Advanced coatings for consolidation of pottery artifacts against deterioration. J Cult Herit. 2023;64:63–72.
9. Salem MZM. Chapter 9—silver nanoparticle applications in wood, wood-based panels, and textiles. In: Abd-Elsalam KA, editor. Silver nanomaterials for agri-food applications. Amsterdam: Elsevier; 2021. p. 219–34.
10. Mazzuca C, Micheli L, Carbone M, Basoli F, Cervelli E, Iannuccelli S, et al. Gellan hydrogel as a powerful tool in paper cleaning process: a detailed study. J Colloid Interface Sci. 2014;416:205–11.
11. Bhardwaj S, Bhardwaj NK, Negi YS. Cleaner approach for improving the papermaking from agro and hardwood blended pulps using biopolymers. J Clean Prod. 2019;213:134–42.
12. Casoli A, Cremonesi P, Isca C, Groppetti R, Pini S, Senin N. Evaluation of the effect of cleaning on the morphological properties of ancient paper surface. Cellulose. 2013;20(4):2027–43.
13. Mazzuca C, Micheli L, Lettieri R, Cervelli E, Coviello T, Cencetti C, et al. How to tune a paper cleaning process by means of modified gellan hydrogels. Microchem J. 2016;126:359–67.
14. Salim E, Abdel-Hamied M, Salim S, Gamal S, Mohamed S, Galal F, et al. Reduction of borax/agar-based gel residues used to neutralize acidity of a historical manuscript with use of different paper barriers: artificial ageing results. BioRes. 2020;15(3):6576–99.
15. Fierascu I, Fierascu RC, Fistos T, Motelica L, Oprea O, Nicoara A, et al. Non-invasive microanalysis of a written page from the Romanian heritage "The Homiliary of Varlaam (Cazania lui Varlaam)." Microchem J. 2021;168: 106345.
16. Abdel-Maksoud G, Emam H, Ragab N. From traditional to laser cleaning techniques of parchment manuscripts: a review. Adv Res Conserv Sci. 2020;1(1):52–76.
17. Abdel-Maksoud G, Abdel-Hamied M, Abou-Elella F, El-Shemy HA. Detection of deterioration for biochemical substances used with late period mummy by GC-MS. Archaeol Anthropol Sci. 2021;13(3):51.
18. Buragohain D, Deka M, Kumar A. Documentation and preservation of endangered manuscripts through digital archiving in North-Eastern states of india. library philosophy and practice. Mizoram: Mizoram University; 2022. p. 1–23.
19. Saha AK. The Conservation of Endangered Archives and Management of Manuscripts in Indian Repositories. Newcastle upon tyne: Cambridge Scholars Publishing; 2020.

20. Zornoza-Indart A, Lopez-Arce P. Silica nanoparticles (SiO2): influence of relative humidity in stone consolidation. J Cul Herit. 2016;18:258–70.
21. Zidan Y, El-Shafei A, Noshy W, Salim E. A comparative study to evaluate conventional and nonconventional cleaning treatments of cellulosic paper supports. Mediterr Archaeol Archaeom. 2017;17(3):337–53.
22. Fornari A, Rossi M, Rocco D, Mattiello L. A review of applications of nanocellulose to preserve and protect cultural heritage wood, paintings, and historical papers. Appl Sci. 2022;12(24):12846.
23. Kołodziejczak-Radzimska A, Jesionowski T. Zinc oxide—from synthesis to application: a review. Materials. 2014;7(4):2833–81.
24. Fallah MH, Fallah SA, Zanjanchi MA. Synthesis and characterization of nano-sized zinc oxide coating on cellulosic fibers: photoactivity and flame-retardancy study. Chin J Chem. 2011;29(6):1239–45.
25. Hassan RRA, Mahmoud SMA, Nessem MA, Abdel Aty RT, Ramzy MG, Dessoky ES, et al. Hydroxypropyl cellulose loaded with ZnO nanoparticles for enhancing the mechanical properties of papyrus (*Cyperus papyrus* L.) strips. BioResources. 2021;16(2):2607–25.
26. Skocaj M, Filipic M, Petkovic J, Novak S. Titanium dioxide in our everyday life; is it safe? Radiol Oncol. 2011;45(4):227–47.
27. Hong T-j, Sivakumar C, Luo C-W, Ho M-S. Investigation of TiO_2 nanoparticle interactions in the fibroblast NIH-3T3 cells via liquid-mode atomic force microscope. Arch Toxicol. 2023;97(11):2893–901.
28. Turner A, Filella M. The role of titanium dioxide on the behaviour and fate of plastics in the aquatic environment. Sci Total Environ. 2023;869: 161727.
29. Musial J, Krakowiak R, Mlynarczyk DT, Goslinski T, Stanisz BJ. Titanium dioxide nanoparticles in food and personal care products—what do we know about their safety? Nanomaterials. 2020;10(6):1110.
30. Toro RG, Diab M, de Caro T, Al-Shemy M, Adel A, Caschera D. Study of the effect of titanium dioxide hydrosol on the photocatalytic and mechanical properties of paper sheets. Materials. 2020;13(6):1326.
31. Arora I, Chawla H, Chandra A, Sagadevan S, Garg S. Advances in the strategies for enhancing the photocatalytic activity of TiO2: conversion from UV-light active to visible-light active photocatalyst. Inorg Chem Commun. 2022;143: 109700.
32. Dell'Edera M, Lo Porto C, De Pasquale I, Petronella F, Curri ML, Agostiano A, et al. Photocatalytic TiO_2-based coatings for environmental applications. Catal Today. 2021;380:62–83.
33. Salama KK, Ali MF, El-Sheikh SM, Nada AA. A new way in synthesizing magnetic nano gel for cleaning an Egyptian Coptic fresco painting. Mediterr Archaeol Archaeom. 2017;17(1):189–189.
34. Sobh RA, Nasr H, Mohamed WS. Synthesis and characterization of magnetic sponge nanocomposite for cleaning archeological lime stones. Egy J Chem. 2020;63(2):507–14.
35. Hassan RRA, Hassan HM, Mohamed YA, Ismail MEM, Farid Y, Mohamed H, et al. ZnO, TiO_2 and Fe_3O_4/Carbopol hybrid nanogels for the cleaner process of paper manuscripts from dust stains and soil remains. Herit Sci. 2023;11(1):221.
36. Gharib A, Maher MA, Ismail SH, Mohamed GG. Effect titanium dioxide/paraloid B. 72 nanocomposite coating on protection of treated Cu-Zn archaeological alloys. Int J Archaeol. 2019;7(2):47–54.
37. Ismail SH, Hamdy A, Ismail TA, Mahboub HH, Mahmoud WH, Daoush WM. Synthesis and characterization of antibacterial carbopol/ZnO hybrid nanoparticles gel. Crystals. 2021;11(9):1092.
38. Hamdy A, Ismail SH, Ebnalwaled AA, Mohamed GG. Characterization of superparamagnetic/monodisperse PEG-coated magnetite nanoparticles sonochemically prepared from the hematite ore for Cd(II) removal from aqueous solutions. J Inorg Organomet Polym Mater. 2021;31(1):397–414.
39. Khalaf MK, Roshdy Elsakhry A, Ismail SH, Abdel-Hamied M, Mohamed GG. Evaluation of nanolime-silica core-shell for consolidation of Egyptian limestone samples with application on an archaeological object. Nano Hybrids Compos. 2022;37:91–102.
40. Ramu AG, Salla S, Gopi S, Silambarasan P, Yang DJ, Song MJ, et al. Surface-tuned hierarchical γ-Fe_2O_3–N-rGO nanohydrogel for efficient catalytic removal and electrochemical sensing of toxic nitro compounds. Chemosphere. 2021;268: 128853.
41. Salem MZM, Hamed SAE-KM, Mansour MMA. Assessment of efficacy and effectiveness of some extracted bio-chemicals as bio-fungicides on wood. Drv Ind. 2019;70(4):337–50.
42. ISO-187. Paper, board and pulps—standard atmosphere for conditioning and testing and procedure for monitoring the atmosphere and conditioning of samples. Geneva: International Organization for Standardization; 1990.
43. Abdel-Maksoud G, Abdel-Hamied M, Abdelhafez AAM. Evaluation of the condition of a Mamluk-illuminated paper manuscript at Al-Azhar Library, Egypt. Pigment Resin Technol. 2023;52(1):49–59.
44. Blinov AV, Nagdalian AA, Arefeva LP, Varavka VN, Kudryakov OV, Gvozdenko AA, et al. Nanoscale composite protective preparation for cars paint and varnish coatings. Coatings. 2022;12(9):1267.
45. Blinov AV, Kachanov MD, Gvozdenko AA, Nagdalian AA, Blinova AA, Rekhman ZA, et al. Synthesis and characterization of zinc oxide nanoparticles stabilized with biopolymers for application in wound-healing mixed gels. Gels. 2023;9(1):57.
46. Ba-Abbad MM, Benamour A, Ewis D, Mohammad AW, Mahmoudi E. Synthesis of Fe3O4 nanoparticles with different shapes through a co-precipitation method and their application. JOM. 2022;74(9):3531–9.
47. Hassan RRA. Behavior of archeological paper after cleaning by organic solvents under heat accelerated ageing. Mediterr Archaeol Archaeomet. 2015;15(3):141–50.
48. Fan H, Li G, Yang F, Yang L, Zhang S. Photodegradation of cellulose under UV light catalysed by TiO_2. J Chem Technol Biotechnol. 2011;86(8):1107–12.
49. Reddy KO, Maheswari CU, Shukla M. Physico-chemical characterization of cellulose extracted from ficus leaves. J Biobased Mater Bio. 2013;7(4):496–9.
50. Hassan RRA, Mohamed WS, Salem MZM, ElMajd AMOA, Ebrahim EEM, Naeem EMA, et al. Cellulose and gellan gum compresses for cleaning mud and pomegranate stains from a historical printed paper. Discov Appl Sci. 2024;6(2):43.
51. Salim E, Ali Hassan RR. Alkyl dimethyl benzyl ammonium chloride as a new cleaner for washing treatments for historical printed paper. Pigment Resin Technol. 2024;53(2):164–72.
52. Reddy KO, Uma Maheswari C, Muzenda E, Shukla M, Rajulu AV. Extraction and characterization of cellulose from pretreated ficus (*Peepal Tree*) leaf fibers. J Nat Fibers. 2016;13(1):54–64.
53. Chalal S, Haddadine N, Bouslah N, Souilah S, Benaboura A, Barille R, et al. Preparation characterization and thermal behaviour of carbopol-TiO_2 nanocomposites. Open J Org Polym Mater. 2014;4(03):55–64.
54. Wang ZG, Zu XT, Xiang X, Yu HJ. Photoluminescence from TiO_2/PMMA nanocomposite prepared by γ radiation. J Nanoparticle Res. 2006;8(1):137–9.
55. Afsharpour M, Imani S. Preventive protection of paper works by using nanocomposite coating of zinc oxide. J Cult Herit. 2017;25:142–8.
56. Afzal S, Samsudin EM, Mun LK, Julkapli NM, Hamid SBA. Room temperature synthesis of TiO_2 supported chitosan photocatalyst: study on physicochemical and adsorption photo-decolorization properties. Mater Res Bull. 2017;86:24–9.

Publisher's Note